



Ligation state of nickel during C–O bond activation with monodentate phosphines

Leidy V. Hooker, Sharon R. Neufeldt*

Department of Chemistry and Biochemistry, Montana State University, 103 Chemistry & Biochemistry Bldg., Bozeman, MT 59717, USA

ARTICLE INFO

Article history:

Received 3 September 2018

Received in revised form

8 October 2018

Accepted 14 October 2018

Available online xxx

Keywords:

DFT

Dispersion

Oxidative addition

Cross coupling

Phosphine ligands

ABSTRACT

The oxidative addition of phenolic electrophiles at Ni(0) in the presence of monodentate phosphine ligands was studied with both dispersion-free and dispersion-containing DFT methods. With the popular bulky ligand PCy₃, consideration of dispersion has a striking effect on the predicted ligation state of nickel during oxidative addition of aryl sulfamates. Dispersion-containing methods such as M06L indicate a clear preference for a bis-phosphine ligated transition state (TS), while dispersion free methods like B3LYP strongly favor a mono-phosphine ligated TS. This discrepancy in predicted ligation state is also found with small phosphines (PM₃) in combination with some aryl electrophiles (carbamates, acetates, pivalates, chlorides), but a bis-PM₃-ligated TS is predicted regardless of dispersion for other electrophiles (sulfamates, mesylates, tosylates). DFT calculations that include dispersion also offer a possible explanation for the observed poor efficacy of P^tBu₃ as a ligand in Ni-catalyzed cross-coupling reactions.

© 2018 Elsevier Ltd. All rights reserved.

1. Introduction

The oxidative addition of phenol derivatives at Ni(0) is a fundamental step of numerous Ni-catalyzed cross coupling reactions [1,2] including Suzuki [3–41], Kumada [3,42–53], Negishi [54–56], Heck [57–59], direct arylations [60–64], and borylation reactions [65–70]. In these cross couplings, nickel is often supported by phosphine ligands. One of the most commonly used phosphines is the bulky monodentate ligand tricyclohexylphosphine (PCy₃), but other highly active systems utilize bidentate ligands. In the latter cases, it is almost certain that nickel is bis-phosphine-ligated during oxidative addition. However, when ligands like PCy₃ are used, the number of phosphines on nickel during this elementary step is not well-established. Correctly modeling nickel's ligation state during oxidative addition is expected to be important for predicting the outcome of Ni-catalyzed cross coupling, especially in situations where selectivity between two or more electrophiles is concerned. Indeed, ligation state is known to have a dramatic influence on the selectivity of analogous oxidative additions at Pd(0) [71–73].

Previous studies on the mechanism of oxidative addition of C–O

bonds at Ni(0) in the presence of bulky monodentate phosphines are limited. Experimental mechanistic studies are hampered by the unavailability of stable Ni(0)[P(alkyl)₃]_n complexes [74]. Several DFT studies have been reported [25,75–82], but only a few explicitly consider both mono- and bis-phosphine ligated transition states (TSs). At least three studies predicted that oxidative addition of aryl acetates, sulfamates, carbamates, and phosphates proceeds preferentially through a NiL—not a NiL₂—TS [25,75,76]. However, dispersion [83] was not considered in these calculations [84]. In contrast, another study examined the oxidative addition of methoxynaphthalene using dispersion-containing DFT (BP86-D3); in this case, a NiL₂ TS was predicted to be favored over the NiL analog [80]. On first consideration, these conflicting results might be attributed to a difference in electrophiles. However, dispersion has repeatedly been shown to play an important role in describing the potential energy surface of reactions involving transition metal catalysts, especially when bulky ligands are involved [85–92]. As such, it is possible that the use of dispersion-containing versus dispersion-free DFT could generally lead to different conclusions about nickel's ligation state during oxidative addition.

Here we compare dispersion-containing and dispersion-free DFT methods for evaluating nickel's ligation state during oxidative addition of C–O bonds with both bulky (PCy₃, P^tBu₃) and small (PM₃) phosphines.

* Corresponding author.

E-mail address: sharon.neufeldt@montana.edu (S.R. Neufeldt).

2. Results and discussion

2.1. Computational studies with $\text{Ni}(\text{PCy}_3)_n$ and phenyl sulfamate

The oxidative addition of phenyl sulfamate **1** at $\text{Ni}(\text{PCy}_3)$ and $\text{Ni}(\text{PCy}_3)_2$ was studied using DFT methods with and without dispersion. Geometries were optimized in the gas phase using either B3LYP [93–95]/BS1 (no dispersion; see Computational Methods for basis set details) or M06L [96]/BS1 (dispersion-containing). Both of these functionals are popular for the study of group 10 organometallic compounds [97]. Energies were further refined by single-point calculations on the optimized geometries using dispersion-containing (M06 [98], M06L, ωB97XD [99], B3LYP-D3BJ [100]; [101]) or dispersion-free (B3LYP, PBE0 [102]) functionals in combination with a large basis set (BS2). In some cases, implicit solvent effects were modeled using the CPCM method (tetrahydrofuran). The conformational complexity of PCy_3 -bearing complexes was considered (see Computational Methods).

Fig. 1 depicts the predicted free energies associated with the reaction of $\text{Ni}(\text{cod})_2$ with **1** and PCy_3 . Geometries and energies were calculated using either dispersion-free (B3LYP, A) or dispersion-containing methods (M06L, B), and final energies were calculated with implicit THF (CPCM). Consistent with previous reports [25,75,76], the dispersion-free method predicts that a NiL_2 pathway is prohibitively high in energy (**Fig. 1A**, black line, **TS3a_{bis3}**), and oxidative addition proceeds through a mono-phosphine-ligated TS (**TS3a_{mono5-O}**, blue line). However, the use of dispersion (**Fig. 1B**) predicts the opposite: a bis-phosphine-ligated TS (**TS3a_{bis3}**) is favored by about 5 kcal mol⁻¹ over the analogous NiL structure **TS3a_{mono5-N}**.

Differences among the calculated transition structures highlight the role of dispersion on geometry optimizations (**Fig. 2**). With M06L, two types of bis-phosphine ligated transition structures can be located. One is a 5-centered TS involving interaction of an S=O oxygen with Ni (**TS3a_{bis5-O}**) [103]. The other resembles a 3-centered oxidative addition TS (**TS3a_{bis3}**), but the Ni···O distance is long (2.92 Å) and the single imaginary frequency corresponds to dissociation of the sulfamate anion away from $[(\text{PCy}_3)_2\text{NiPh}]$. IRC calculations on a smaller model system also suggest that there is little interaction between Ni and O in this TS:

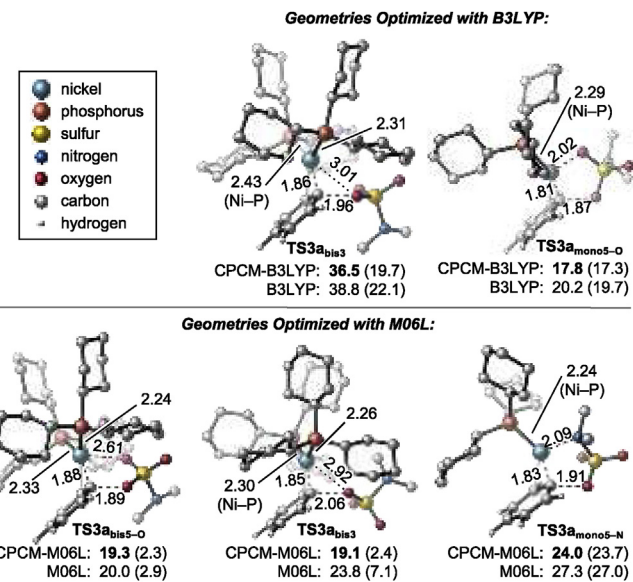


Fig. 2. Transition structures (TS3a) for oxidative addition of phenyl sulfamate **1** at $\text{Ni}(\text{PCy}_3)_n$ ($n = 1$ or 2). Structures were optimized using either B3LYP/BS1 (top) or M06L/BS1 (bottom). Single point Gibbs free energies and enthalpies (in parentheses) calculated with B3LYP/BS2 (top) or M06L/BS2 (bottom) are provided with solvent correction [CPCM (THF)] and also in the gas phase. Energy units are kcal mol⁻¹. Bond distances are in angstroms. Most hydrogens are hidden for clarity.

this Ni···O distance initially elongates along the IRC after the TS (see Supporting Information for details). As such, **TS3a_{bis3}** more closely resembles an $S_N\text{Ar}$ mechanism for oxidative addition [104]. Consistent with increased charge separation in **TS3a_{bis3}**, this TS is higher energy than **TS3a_{bis5}** in the gas phase (23.8 vs. 20.0 kcal mol⁻¹), but slightly more stable in THF (19.1 v.s 19.3 kcal mol⁻¹). A similar trend is calculated with a tosylate leaving group (see Supporting Information). With B3LYP, only the $S_N\text{Ar}$ -type TS (**TS3a_{bis3}**) can be located: apparently, a 5-centered TS is too sterically crowded when London dispersion forces are ignored. The phosphine ligands are closer to Ni in the NiL_2 transition structures calculated with M06L than with B3LYP because M06L accounts for

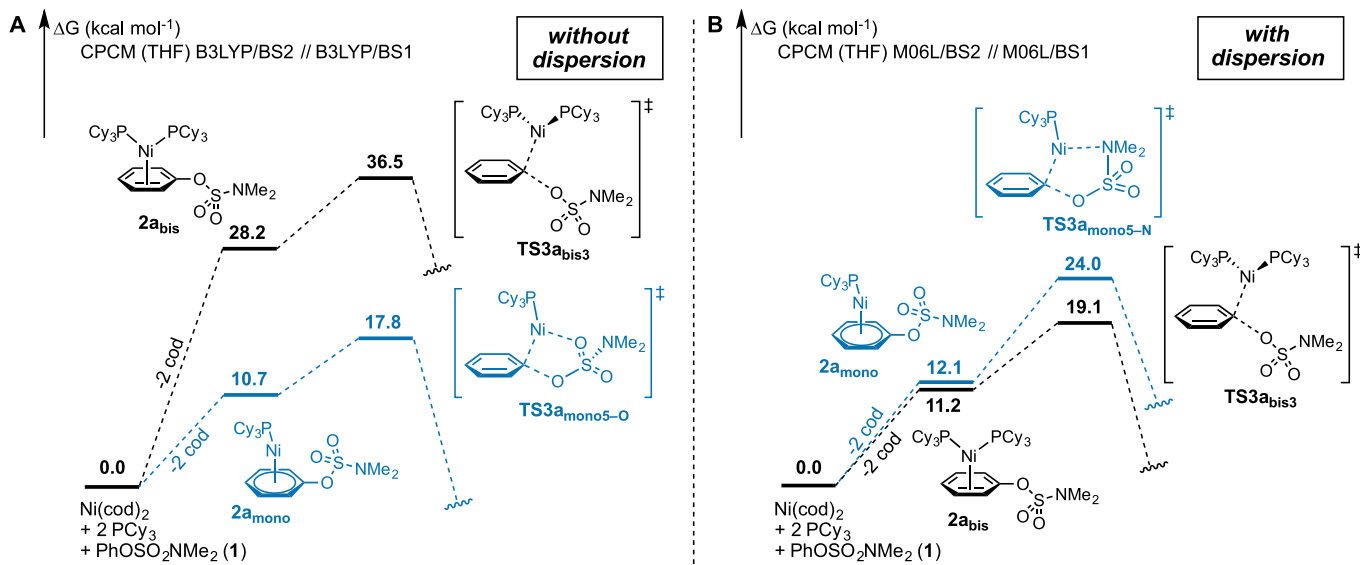


Fig. 1. Calculated reaction pathway for oxidative addition of phenyl sulfamate **1** at $\text{Ni}(\text{PCy}_3)_n$ ($n = 1$ or 2) using (A) a dispersion-free method or (B) a dispersion-containing method. Energies are Gibbs free energies in kcal mol⁻¹.

attractive van der Waals interactions. With a single PCy₃ ligand, M06L predicts that a 5-centered TS involving a Ni···N interaction (**TS3a_{mono5-N}**) is lower energy than one involving a Ni···O interaction. Conversely, B3LYP favors a Ni···O interaction (**TS3a_{mono5-O}**), likely because nitrogen is more sterically hindered than oxygen.

We next considered the role of solvent and the use of other functionals on the predicted preference for mono-vs. bis-ligation. As illustrated in Fig. 3, the calculated free energy difference between NiL₂ and NiL transition structures is largely independent of solvent for both dispersion-free and dispersion-containing methods (compare entry 1 with 2, and entry 5 with 6). Regardless of whether geometries were optimized with or without dispersion (M06L vs. B3LYP), single point energy calculations using functionals that do not consider dispersion (B3LYP, PBE0) predict that a monoligated TS is strongly favored (entries 1–4). In contrast, energy calculations with dispersion-corrected methods (M06L, M06, ωB97XD, B3LYP-D3BJ) consistently predict that a bisligated TS is preferred (entries 5–10).

Although numerous reports suggest that dispersion-corrected methods are more accurate than dispersion-free [85–91,105–122], there have also been instances in which dispersion appears to be overestimated [123–125]. As such, it is difficult to say which of the two contradictory predictions about nickel's ligation state with PCy₃ should be believed. The following sections describe further studies to evaluate the differences between these two classes of methods.

2.2. Computational studies with Ni(PMe₃)_n

As described above, dispersion-containing methods predict that oxidative addition of phenyl sulfamate is significantly easier at Ni(PCy₃)₂ than at Ni(PCy₃), while dispersion-free methods predict

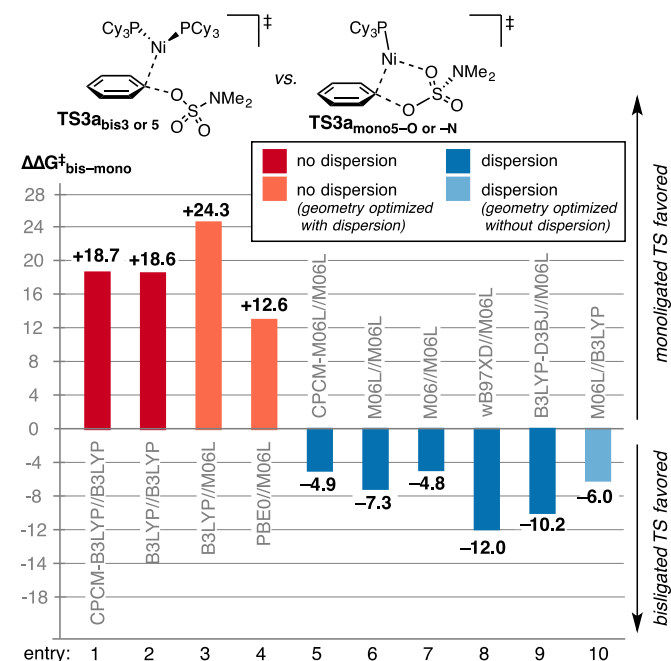


Fig. 3. Gibbs free energy differences between bis-PCy₃-ligated and mono-PCy₃-ligated transition structures for oxidative addition of phenyl sulfamate **1** at Ni(0). Values are in kcal mol⁻¹. In the method//method nomenclature, the first term indicates the method used for single-point energy calculations and the second term indicates the method used for geometry optimizations. Where indicated, the CPCM method was used for implicit solvent (THF). Geometry optimizations were conducted with BS1, and single point energy calculations were conducted with BS2.

the opposite. To evaluate the extent to which this discrepancy depends on ligand bulk, we next calculated pathways for oxidative addition of **1** at Ni(PMe₃)_n (Fig. 4). In contrast to the results with PCy₃, dispersion-free and dispersion-containing methods give qualitatively similar results with PMe₃. Both predict a bisphosphine-ligated transition state. Nevertheless, the magnitude to which the NiL₂ pathway is favored varies substantially between the two methods ($\Delta\Delta G^\ddagger_{\text{bis-mono}} = -5.4$ vs. $-10.0 \text{ kcal mol}^{-1}$ for B3LYP and M06L, respectively). Unlike the results with PCy₃, a 5-centered bis-phosphine-ligated TS (**TS3b_{bis5}**, $\Delta G^\ddagger = 16.7 \text{ kcal mol}^{-1}$) is slightly more favorable than a S_NAr-type TS ($\Delta G^\ddagger = 17.3 \text{ kcal mol}^{-1}$, not shown) when calculated using M06L. However, the reverse is true when B3LYP is used ($\Delta G^\ddagger = 12.8 \text{ kcal mol}^{-1}$ for a 5-centered TS [not shown] vs. $9.5 \text{ kcal mol}^{-1}$ for the S_NAr **TS3b_{bis3}**).

Consistent with the results using **1**, a Ni(PMe₃)₂ pathway is predicted for the oxidative addition of related sulfonates using both dispersion-containing and dispersion-free methods. As shown in Fig. 5 for the reaction of phenyl mesylate **4** and phenyl tosylate **5**, TS energies calculated with both B3LYP and M06L are lower for bisligated nickel (orange and light blue) than monoligated (red and dark blue columns). In contrast, carbonyl-containing electrophiles **6–8** are predicted by B3LYP calculations to react through monoligated TSs (red columns) and aryl chlorides (**9**) are predicted to show no preference for mono-vs. bis-ligated transition structures. Overall, with the small ligand PMe₃, the dispersion-free prediction about nickel's ligation state depends on the electrophile. On the other hand, when dispersion is considered (M06L), a bis-ligated transition state is always favored regardless of electrophile (compare dark and light blue columns). Interestingly, both methods predict nearly the same reactivity order for this series of electrophiles with PMe₃, despite differences in the predicted ligation state of nickel.

2.3. Experimental and computational studies with P(^tBu)₃, PCy₃, and PMe₃

Based on our calculations with PCy₃ and PMe₃, predictions made with dispersion-containing and dispersion-free methods diverge more significantly with bulkier ligands. In an effort to clarify which method is more accurate, we next compared B3LYP vs. M06L predictions with an even more hindered ligand, P^tBu₃. In palladium-catalyzed cross-couplings of aryl halides, bulky monodentate ligands—most notably P^tBu₃—are particularly efficient [126]. One proposed rationale for the efficacy of bulky ligands is that they promote oxidative addition via mono-phosphine ligated palladium [127]. In contrast, examples of efficient Ni/P^tBu₃ systems for cross-coupling are notably absent from the literature [6,54,80]. Indeed, in our own hands, the use of P^tBu₃ in combination with Ni(cod)₂ provides only trace product under conditions that are effective for Suzuki cross coupling of **10** using PCy₃ (Table 1). This poor reactivity appears to originate in the oxidative addition step of catalysis. In a stoichiometric experiment, **12** reacts with Ni(cod)₂ and PCy₃ to form the oxidative addition product **13** (Fig. 6A) [128]. In contrast, no reaction is observed when P^tBu₃ is used (Fig. 6B) [129]. We were interested in whether either B3LYP or M06L calculations could shed light on the poor efficacy of P^tBu₃.

Unlike the calculated results with PCy₃, M06L predicts that the bis-P^tBu₃-ligated reaction pathway is prohibitively high in energy (Fig. 7B, black line, **TS3c_{bis3}**). The mono-ligated pathway is instead favored according to this method (blue line, **TS3c_{mono5-N}**). However, this mono-ligated transition state has a calculated free energy of 26.0 kcal mol⁻¹ measured from separated reactants. This barrier is large when compared to the predicted barrier for reaction with PCy₃ (**TS3a_{bis3}**, Fig. 1, 19.1 kcal mol⁻¹). As such, these calculations

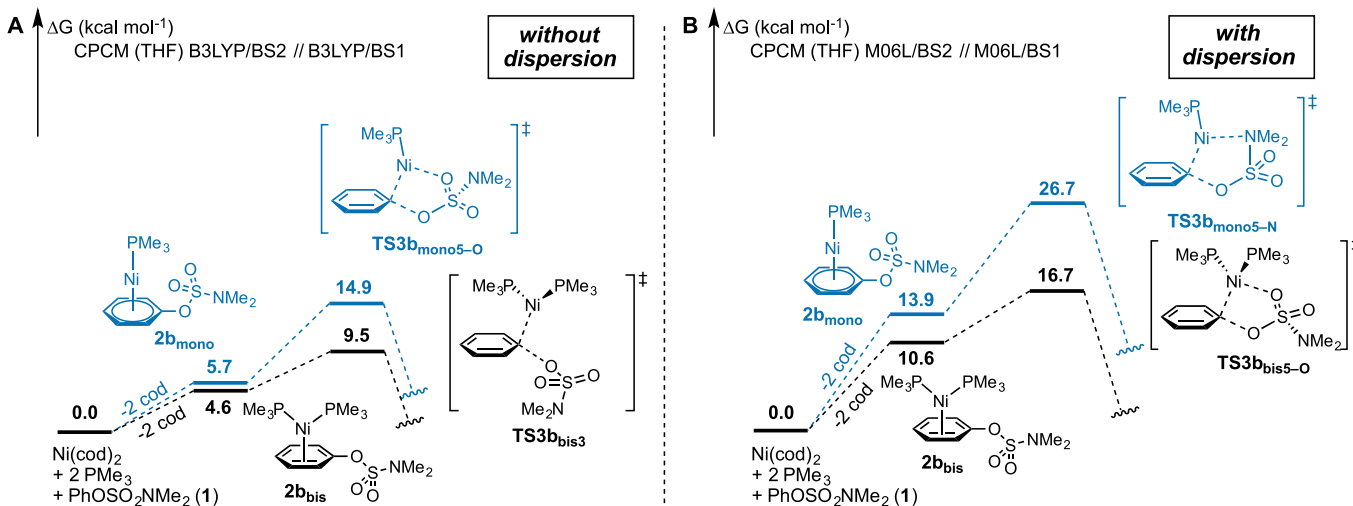


Fig. 4. Calculated reaction pathway for oxidative addition of phenyl sulfamate **1** at $\text{Ni}(\text{PMe}_3)_n$ ($n = 1$ or 2) using (A) a dispersion-free method or (B) a dispersion-containing method. Energies are Gibbs free energies in kcal mol⁻¹.

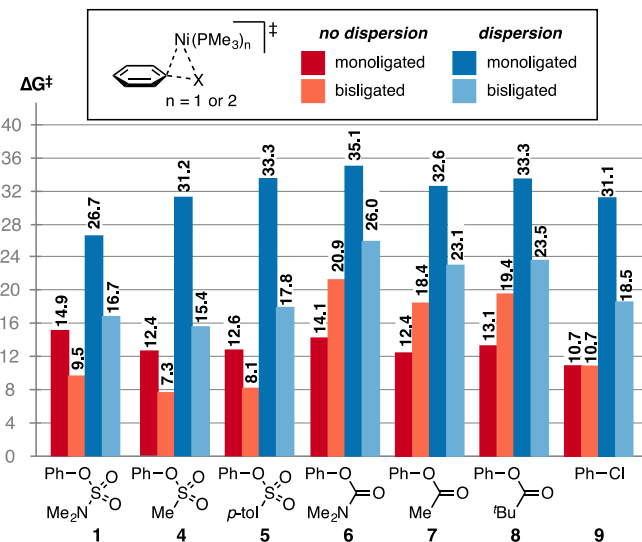
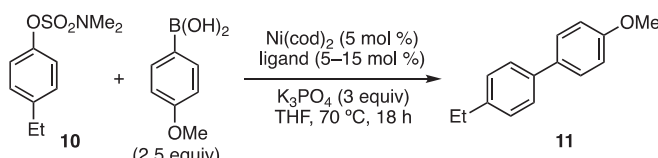


Fig. 5. Minimum transition structure energies for oxidative addition of various electrophiles (**1**, **4–9**) at $\text{Ni}(\text{PMe}_3)_n$ ($n = 1$ or 2), calculated with a dispersion free [CPCM (THF) B3LYP/BS2//B3LYP/BS1, red and orange] or dispersion-corrected method [CPCM (THF) M06L/BS2//M06L/BS1, dark and light blue]. Gibbs free energies are in kcal mol⁻¹.

Table 1

Ni-catalyzed Suzuki cross coupling of an aryl sulfamate using monodentate phosphine ligands.



Entry	ligand (mol %)	10 (%) ^a	11 (%) ^a
1	PCy_3 (10)	2.6(1)	86(11)
2	P^tBu_3 (5)	79(9)	16(1)
3	P^tBu_3 (10)	79(7)	13(1)
4	P^tBu_3 (15)	88(11)	11(1)

^a Average of three GC calibrated yields (standard deviation).

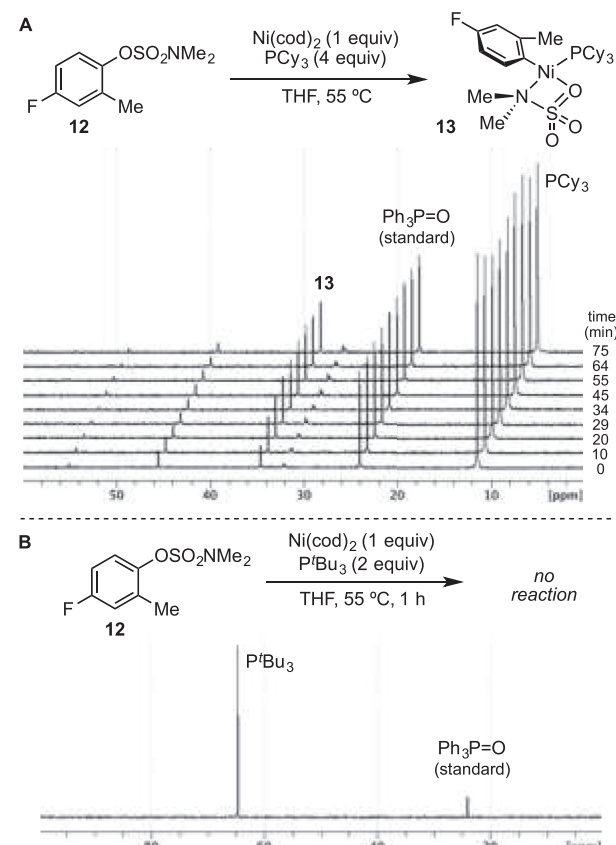


Fig. 6. (A) Stoichiometric reaction of $\text{Ni}(\text{cod})_2$ and PCy_3 with aryl sulfamate **12**. Stacked ^{31}P NMR spectra show progression over ~75 min. (B) No reaction is observed between $\text{Ni}(\text{cod})_2$, P^tBu_3 , and **12** after 1 h.

are consistent with the observed poor reactivity of $\text{Ni}/\text{P}^t\text{Bu}_3$ compared to Ni/PCy_3 with **10** and **11**.

Using B3LYP, we were unable to locate a transition state **TS3cbis3** for oxidative addition of $\text{Ni}(\text{P}^t\text{Bu}_3)_2$ into **1**. This outcome is consistent with Schoenebeck's calculations on palladium-based systems: dispersion is also required to locate oxidative addition transition

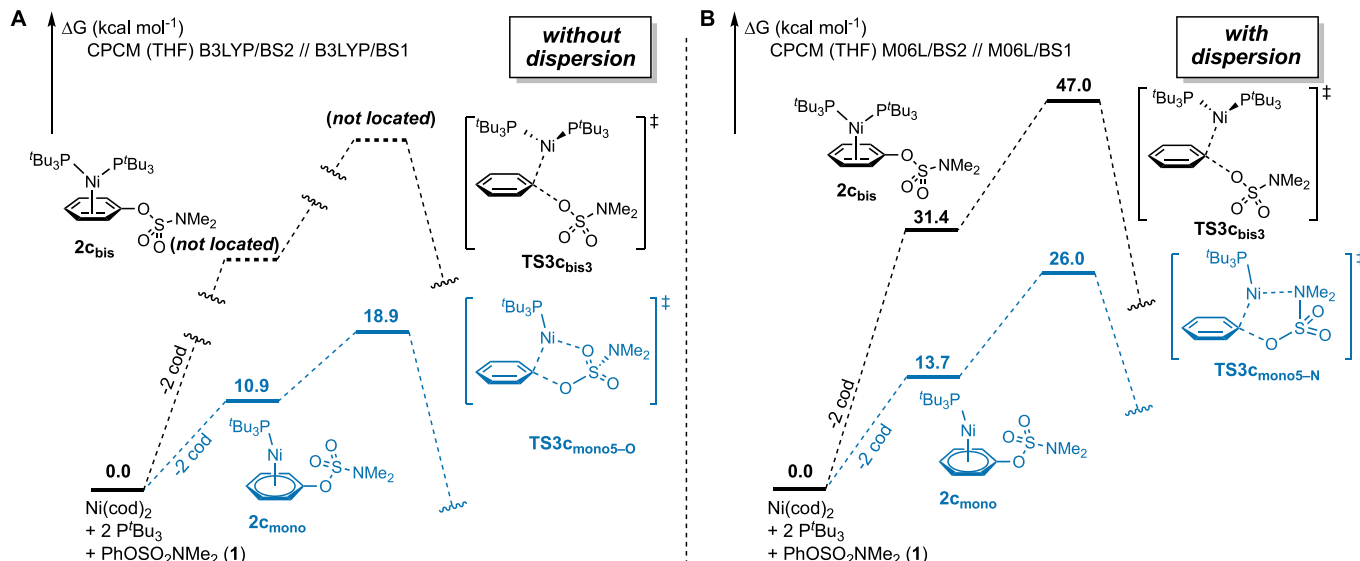


Fig. 7. Calculated reaction pathway for oxidative addition of phenyl sulfamate **1** at $\text{Ni}(\text{P}'\text{Bu}_3)_n$ ($n = 1$ or 2) using (A) a dispersion-free method or (B) a dispersion-containing method. Energies are Gibbs free energies in kcal mol^{-1} .

states using $\text{Pd}(\text{P}'\text{Bu}_3)_2$ [92]. The dispersion-free calculations predict that oxidative addition at $\text{Ni}(\text{P}'\text{Bu}_3)$ should have a nearly identical barrier to that calculated with $\text{Ni}(\text{PCy}_3)$ when measured from separated reactants (18.9 and 17.8 kcal mol^{-1} for $\text{TS3c}_{\text{mono}5-\text{O}}$ and $\text{TS3a}_{\text{mono}5-\text{O}}$, respectively). This result does not appear to be consistent with the experimentally observed lack of reactivity of $\text{Ni}/\text{P}'\text{Bu}_3$. Nevertheless, we cannot rule out the possibility that the poor reactivity of $\text{Ni}/\text{P}'\text{Bu}_3$ is due to other factors that are more challenging to model such as slow substitution of cod for $\text{P}'\text{Bu}_3$ when $\text{Ni}(\text{cod})_2$ is employed [130].

Overall, consideration of dispersion provides results that may explain the poor reactivity of $\text{Ni}/\text{P}'\text{Bu}_3$ toward oxidative addition. Using M06L, this elementary step is predicted to be generally much easier when nickel is ligated by two phosphines. A bis-ligated TS is accessible with PCy_3 (and PMMe_3), but prohibitively high in energy with $\text{P}'\text{Bu}_3$. With $\text{P}'\text{Bu}_3$, oxidative addition can only take place through a mono-phosphine-ligated TS that has an associated high energy barrier [131]. If this explanation for the inefficacy of $\text{P}'\text{Bu}_3$ is correct, it suggests that dispersion-containing DFT methods are better able to reproduce experiment. This conclusion fits with a growing body of literature indicating that dispersion is critical to the accurate modeling of organometallic compounds [85–92]. In this case, consideration of dispersion predicts that oxidative addition is favored at NiL_2 over NiL for ligands as bulky as PCy_3 [34], in contrast to predictions made using dispersion-free methods [25,75,76]. Nevertheless, further experiments will be needed to verify that dispersion-containing methods do not over-estimate the stability of NiL_2 transition states.

3. Conclusions

This work demonstrates that dispersion-containing and dispersion-free DFT provide different predictions about nickel's ligation state by bulky phosphines during oxidative addition of phenolic electrophiles. With PCy_3 as the ligand, dispersion-containing methods predict that oxidative addition of phenyl sulfamate is favored at NiL_2 over NiL by ~5–12 kcal mol^{-1} . Dispersion-free DFT predicts the opposite, indicating that reaction at NiL is favored by ~12–24 kcal mol^{-1} . The conflicting predictions of these two DFT method classes are notable, as each suggests that different

ligation states are favored by energy values larger than normal acceptable error. When considering a small phosphine ligand (PMMe_3), a bis-ligated TS for oxidative addition of aryl sulfamates, mesylates, and tosylates is predicted regardless of dispersion correction. However, dispersion and dispersion-free methods disagree about the number of PMMe_3 ligands on nickel during reaction of carbonyl-containing electrophiles (carbamates, acetates, pivalates). As such, dispersion can affect ligation state predictions for both bulky and small phosphines, although this effect is more dramatic with bulky ligands.

Which predictions are correct? Numerous reports suggest that consideration of dispersion is critical to accurately modeling many organic and organometallic reactions [85–91,105–122]. If oxidative addition of phenolic electrophiles at $\text{Ni}(0)$ fits the literature trend, then it is likely that this elementary step proceeds through a NiL_2 TS as predicted with dispersion-containing DFT, even with monodentate ligands as bulky as PCy_3 . Calculations using M06L—but not B3LYP—also offer a possible explanation for the poor reactivity of $\text{P}'\text{Bu}_3$. With this especially hindered ligand, both M06L and B3LYP predict that a NiL pathway is lower energy than one involving NiL_2 . However, B3LYP predicts a similar barrier for oxidative addition using $\text{P}'\text{Bu}_3$ and PCy_3 , because mono-ligated transition structures are generally favorable when dispersion is ignored. In contrast, M06L predicts a much higher barrier with $\text{P}'\text{Bu}_3$ because NiL transition structures are generally unstable when dispersion is considered. Further experimental studies are underway to evaluate the accuracy of these predictions.

4. Computational methods

Calculations were performed with Gaussian 09 [132]. An ultra-fine integration grid and the keyword 5d were used for all calculations. Geometry optimizations of stationary points were carried out in the gas phase with the M06L [96] or B3LYP [93–95] functional with the LANL2DZ [133] pseudopotential for Ni and the 6-31G(d) basis set for all other atoms (BS1). Frequency analyses were carried out at the same level to evaluate the zero-point vibrational energy and thermal corrections at 298 K. Cramer and Truhlar's anharmonic correction was applied to frequencies that are less than 100 cm^{-1} [134]. The nature of the stationary points was determined

in each case according to the appropriate number of negative eigenvalues of the Hessian matrix. Forward and reverse intrinsic reaction coordinate (IRC) calculations were carried out on representative optimized transition structures to ensure that the TSs indeed connect the appropriate reactants and products [135–137]. Multiple conformations were considered for all structures when applicable. In particular, the conformational complexity of PCy₃ was considered as follows: First, an initial input geometry of free PCy₃ was obtained from the crystal structure of Ni(PCy₃)₂(C₂H₄)₂ [138]. Three additional conformations of this ligand were also considered. With both B3LYP and M06L, the lowest energy optimized geometry of PCy₃ corresponded to that of the crystal structure. This geometry was used as the basis for building PCy₃-ligated Ni structures. Three and nine conformations were considered as input structures for the geometry optimizations of NiL and NiL₂ complexes, respectively. Only the lowest energy conformations are reported herein. Single point energies calculations were performed on the gas-phase optimized geometries using the indicated functional with the SDD [139,140] pseudopotential for Ni and the 6-311++G(2d,p) basis set for all other atoms. Where indicated, bulk solvent effects in tetrahydrofuran were considered implicitly in the single point energy calculations through the CPCM continuum solvation model [141]. Images of optimized structures were generated with CYLview [142].

5. Experimental methods

5.1. General

NMR spectra were obtained on a Bruker 500 (500.232 MHz for ¹H, 125.795 MHz for ¹³C) spectrometer. ¹H and ¹³C NMR chemical shifts are reported in parts per million (ppm) relative to TMS, with the residual solvent peak used as an internal reference. ³¹P chemical shifts are reported in ppm relative to phosphoric acid, with Ph₃PO used as an internal or external reference. Multiplicities are reported as follows: singlet (s), doublet (d), doublet of doublets (dd), doublet of doublets of doublets (ddd), triplet (t), quartet (q), multiplet (m), and broad resonance (br).

5.2. Materials

Tricyclohexylphosphine (PCy₃), triphenylphosphine oxide, 4-methoxybenzeneboronic acid, and 4-fluoro-2-methylphenol were obtained from Oakwood Chemical and used as received. Potassium phosphate, Ni(cod)₂, dimethylsulfamoyl chloride, sodium hydride (60% dispersion in oil) and 4-ethylphenol were obtained from Acros and used as received. P^tBu₃ was obtained from Alfa Aesar and was used as received. Phosphoric acid, diethyl ether, and ethyl acetate were obtained from Fisher and used as received. THF and toluene were obtained from Fisher and were degassed and dried with a JC Meyer solvent system before use. Hexanes was obtained from Fisher and was used as received or degassed by freeze-pump-thaw for isolation of oxidative addition complex **13**. Benzene-d₆ and D₂O were obtained from Cambridge Isotope Laboratories and used as received. Flash column chromatography was performed on SiliCycle silica gel 60 (40–63 µm particle size) and thin layer chromatography was performed on SiliCycle TLC plates pre-coated with extra hard silica gel 60 F₂₅₄.

5.3. Synthesis and characterization of substrates

5.3.1. 4-Ethylphenyl sulfamate (**10**)

Compound **10** was prepared by a procedure adapted from the literature [13]. To an oven-dried 250 mL round bottom flask was added NaH (0.431 g, 10.76 mmol, 1.2 equiv). The flask was sealed

with a septum and flushed with N₂. To an oven-dried 50 mL round bottom flask was added 4-ethylphenol (1.1 g, 8.97 mmol, 1.0 equiv) and DME (24 mL). The 50 mL flask was degassed and the contents transferred to the 250 mL flask via cannula at 0 °C. Upon completion of the addition of 4-ethylphenol, the 250 mL flask was warmed to room temperature for 10 min and then returned to an ice bath. To an oven-dried 25 mL round bottom flask was added dimethylsulfamoyl chloride (1 mL, 10.76 mmol, 1.2 equiv). The 25 mL flask was degassed and the contents transferred to the 250 mL flask via cannula at 0 °C. The 250 mL reaction flask was then warmed to room temperature and allowed to stir overnight. The reaction was quenched with ~5 mL H₂O and concentrated under vacuum. The resulting crude was then dissolved in Et₂O (50 mL) and H₂O (15 mL) and transferred to a separatory funnel. The layers were separated and the organic layer was washed with 1 M KOH (15 mL) and H₂O (15 mL). The combined aqueous layers were extracted with Et₂O (3 × 20 mL). The combined organic layers were washed with brine (15 mL), dried over MgSO₄, and concentrated under vacuum. The crude product was purified by column chromatography on silica gel (R_f = 0.7 in benzene) to yield **10** as a pale yellow oil (0.842 g, 41% yield). Yield is low because of co-elution of an impurity. ¹H NMR (acetone-d₆): δ 7.29 (d, J = 8.8 Hz, 2H), 7.23 (d, J = 8.8 Hz, 2H), 2.95 (s, 6H), 2.66 (q, J = 7.6 Hz, 2H), 1.21 (t, J = 7.6 Hz, 3H). ¹³C{¹H} NMR (acetone-d₆): δ 149.4, 143.8, 130.0, 122.7, 39.0, 28.8, 16.1. HRMS Calcd for C₁₀H₁₆SO₃N⁺ 230.0845; found: 230.0863.

5.3.2. 4-Fluoro-2-methylphenyl sulfamate (**12**)

Compound **12** was prepared by a procedure adapted from the literature [13]. To an oven-dried 250 mL round bottom flask was added NaH (0.44 g, 10.8 mmol, 1.2 equiv). The flask was sealed with a septum and flushed with N₂. To an oven-dried 50 mL round bottom flask was added 4-fluoro-2-methylphenol (1.135 g, 9.00 mmol, 1.0 equiv) and DME (24 mL). The 50 mL flask was degassed and the contents transferred to the 250 mL flask via cannula at 0 °C. Upon completion of the addition of 4-fluoro-2-methylphenol, the 250 mL flask was warmed to room temperature for 10 min and then returned to an ice bath. To an oven-dried 25 mL round bottom flask was added dimethylsulfamoyl chloride (1.15 mL, 10.8 mmol, 1.2 equiv). The 25 mL flask was degassed and the contents transferred to the 250 mL flask via cannula at 0 °C. The 250 mL flask was then warmed to room temperature and allowed to stir overnight. The reaction was quenched with ~5 mL H₂O and concentrated under vacuum. The resulting crude material was then dissolved in Et₂O (50 mL) and H₂O (15 mL) and transferred to a separatory funnel. The layers were separated and the organic layer was washed with 1 M KOH (15 mL) and H₂O (15 mL). The combined aqueous layers were extracted with Et₂O (3 × 20 mL). The combined organic layers were washed with brine (15 mL), dried over MgSO₄, and concentrated under vacuum. The crude product was purified by recrystallization from 97% hexanes/3% ethyl acetate to yield **12** as a white solid (1.66 g, 79% yield). ¹H NMR (acetone-d₆): δ 7.33 (dd, J = 8.8, 5.0 Hz, 1H), 7.11 (dd, J = 9.2, 3.1 Hz, 1H), 7.02 (ddd, J = 8.8, 8.5, 3.1 Hz, 1H), 3.05 (s, 6H), 2.36 (s, 3H). ¹³C{¹H} NMR (C₆D₆): δ 161.2 (d, J = 245 Hz), 145.3 (d, J = 2.7 Hz), 134.2 (d, J = 8.4 Hz), 124.2 (d, J = 9.1 Hz), 118.5 (d, J = 22.8 Hz), 114.0 (d, J = 23.5 Hz), 38.5, 16.8. ¹⁹F NMR (C₆D₆): δ -116.2 (m). HRMS Calcd for C₉H₁₃SO₃NF⁺ 234.0595; found: 234.0590.

5.4. Catalytic cross coupling (*Table 1*)

5.4.1. General procedure

In a nitrogen atmosphere glove box, **10** (22.9 mg, 0.1 mmol, 1.0 equiv), K₃PO₄ (63.7 mg, 0.3 mmol, 3.0 equiv), and 4-methoxybenzeneboronic acid (53.1 mg, 0.25 mmol, 2.5 equiv) were combined in a 4 mL scintillation vial equipped with a

magnetic stir bar. To this vial were added stock solutions of $\text{Ni}(\text{cod})_2$ and ligand in THF. Stock solutions were prepared as follows: (A) For reactions using PCy₃: $\text{Ni}(\text{cod})_2$ (2.7 mg, 0.010 mmol), PCy₃ (5.6 mg, 0.020 mmol), and THF (0.6 mL); 0.3 mL of this stock solution was transferred to a vial containing **10**. (B) For reactions using P^tBu₃: $\text{Ni}(\text{cod})_2$ (5.5 mg, 0.020 mmol) and THF (0.4 mL) were combined in one vial; 0.1 mL of this stock solution was transferred to a vial containing **10**. P^tBu₃ (9.1 mg, 0.045 mmol) and THF (0.6 mL) were combined in another vial; 0.2, 0.1, or 0.05 mL of this stock solution was transferred to a vial containing **10**. When applicable, additional THF was added to bring the total volume to 0.3 mL. The reaction vial was sealed with a PTFE-lined cap and removed from the glove box where it was allowed to stir (750 rpm) at 70 °C for 18 h. Undecane (10.5 μL , 0.5 equiv) was then added as an internal GC standard and the vial was diluted with ~3.7 mL Et₂O and mixed well. An aliquot was filtered through celite and analyzed by GC.

5.4.2. 4-Methoxy-4'-ethylbiphenyl (**11**)

In a nitrogen atmosphere glove box, **10** (229.3 mg, 1 mmol, 1.0 equiv), K₃PO₄ (636.8 mg, 3 mmol, 3.0 equiv), and 4-methoxybenzeneboronic acid (379.9 mg, 2.5 mmol, 2.5 equiv) were combined in a 4 mL scintillation vial equipped with a magnetic stir bar. In a separate vial, $\text{Ni}(\text{cod})_2$ (13.8 mg, 0.05 mmol, 5 mol %), PCy₃ (28 mg, 0.1 mmol, 10 mol%), and THF (3.0 mL) were allowed to stir until fully dissolved. The solution of nickel and ligand was then transferred by pipette to the vial containing **10**. The reaction vial was sealed with a PTFE-lined cap and removed from the glove box where it was allowed to stir (750 rpm) at 70 °C for 18 h. The crude reaction was diluted with Et₂O, filtered through celite, and the celite was rinsed with copious Et₂O. The filtrate was concentrated under vacuum, and the crude residue was purified by column chromatography on silica gel ($R_f = 0.5$ in 80% hexanes/20% benzene) to yield compound **11** as a white solid (139.8 mg, 66%). ¹H NMR (acetone-*d*₆): δ 7.56 (d, *J* = 8.9 Hz, 2H), 7.51 (d, *J* = 8.3 Hz, 2H), 7.27 (d, *J* = 8.3 Hz, 2H), 7.00 (d, *J* = 8.9 Hz, 2H), 3.83 (s, 3H), 2.66 (q, *J* = 7.6 Hz, 2H), 1.24 (t, *J* = 7.6 Hz, 3H). ¹³C{¹H} NMR (acetone-*d*₆): δ 160.3, 143.6, 139.1, 134.4, 129.3, 128.7, 127.4, 115.2, 55.7, 29.2, 16.2. The spectroscopic data are consistent with those reported in the literature [143].

5.5. Stoichiometric NMR studies (Fig. 6)

In a nitrogen atmosphere glove box, **12** (4.7 mg, 0.02 mmol, 1 equiv) was combined with THF (0.2 mL) in a 4 mL vial. In a separate vial, $\text{Ni}(\text{cod})_2$ (5.5 mg, 0.02 mmol, 1 equiv), THF (0.5 mL), and either PCy₃ (22.4 mg, 0.08 mmol, 4 equiv) or P^tBu₃ (8.1 mg, 0.04 mmol, 2 equiv) were allowed to stir until fully dissolved. The solutions of **12** and of nickel and ligand were then transferred into an NMR tube. A capillary tube containing an NMR standard of Ph₃PO in benzene-*d*₆ (0.1 mL) was added to the NMR tube. The opening of the NMR tube was covered with PTFE tape and capped before it was removed from the glovebox. Upon removal from the glovebox, the NMR tube was frozen in liquid nitrogen before transporting to the NMR instrument. The NMR spectrometer was warmed to 55 °C and ³¹P spectra were acquired at regular intervals until no further change was observed (PCy₃) or for one hour (P^tBu₃).

5.6. Synthesis, isolation, and characterization of oxidative addition complex **13**

5.6.1. [(PCy₃)Ni(4-fluoro-2-methylphenyl)(OSO₂NMe₂)] **13**

In a nitrogen atmosphere glovebox, $\text{Ni}(\text{cod})_2$ (137.5 mg, 0.5 mmol, 1 equiv), PCy₃ (560.9 mg, 2 mmol, 4 equiv), **12** (116.6 mg, 0.5 mmol, 1 equiv), and THF (2.5 mL) were combined in a 4 mL scintillation vial, sealed with a PTFE-lined cap, and allowed to stir at

room temperature overnight. The crude reaction mixture was concentrated under vacuum to provide a burnt orange residue. In the glovebox, the crude residue was washed with degassed hexanes six times. The remaining residue was dried under vacuum to yield product **13** as a burnt orange solid (103.6 mg, 36%). X-ray quality crystals were grown from toluene/pentane at -25 °C. ¹H NMR (C₆D₆): δ 7.09 (dd, *J* = 8.5, 6.8 Hz, 1H), 6.64–6.57 (multiple signals, 2H), 3.13 (s, 3H), 2.54 (br, 3H), 2.07–2.04 (multiple signals, 6H), 1.70–1.46 (multiple signals, 18H) 1.41–1.33 (m, 3H), 1.08–0.97 (m, 6H), 0.91–0.84 (m, 3H). ¹³C{¹H} NMR (C₆D₆): δ 162.0 (d, *J* = 240.1 Hz), 144.7 (d, *J* = 5.5 Hz), 136.5 (d, *J* = 5.1 Hz), 132.1 (d, *J* = 38.4 Hz), 114.2 (d, *J* = 16.4 Hz), 110.5 (d, *J* = 17.4 Hz), 42.0 (br), 41.3 (br), 33.3 (d, *J* = 21.1 Hz), 30.1, 28.9 (d, *J* = 1.8 Hz), 27.4 (d, *J* = 11.0 Hz), 27.2 (d, *J* = 10.1 Hz), 26.2 (d, *J* = 2.3 Hz), 26.1. ¹⁹F NMR (C₆D₆): δ -123.5 (m). ³¹P{¹H} NMR (C₆D₆): δ 34.6 (s).

5.6.2. Crystal data and structural refinement for **13**

X-ray diffraction data for **13** were collected at 100 K on a Bruker D8 Venture using MoK α -radiation ($\lambda = 0.71073 \text{ \AA}$). Data have been corrected for absorption using SADABS [144] area detector absorption correction program. Using Olex2 [145], the structure was solved with the SHELXT [146] structure solution program using Direct Methods and refined with the SHELXL [147] refinement package using least squares minimization. All non-hydrogen atoms were refined with anisotropic thermal parameters. Hydrogen atoms in the investigated structure were placed in geometrically calculated positions and refined using a riding model. Isotropic thermal parameters of the placed hydrogen atoms were fixed to 1.2 times the U value of the atoms they are linked to (1.5 times for methyl groups). The phenyl and dimethylaminosulfonate ligands display disorder and have been modeled over two positions using a PART instruction and tied to a single free variable. Refinement of the free variable shows an approximate 80:20 disorder. Bond and thermal ellipsoid similarity restraints, as well as 5 EADP constraints were used to model the second position of the two ligands. Calculations and refinement of structures were carried out using APEX3 [148], SHELXTL [149], and Olex2 software. Empirical formula: C₂₇H₄₅FNNiO₃PS ($M = 572.38 \text{ g/mol}$): orthorhombic, space group $P2_12_12_1$ (no. 19), $a = 10.0593(8) \text{ \AA}$, $b = 15.6615(14) \text{ \AA}$, $c = 17.8546(18) \text{ \AA}$, $V = 2812.9(4) \text{ \AA}^3$, $Z = 4$, $T = 100 \text{ K}$, $\mu(\text{MoK}\alpha) = 0.856 \text{ mm}^{-1}$, $D_{\text{calc}} = 1.352 \text{ g/cm}^3$, $2\theta_{\text{max}} = 54.966^\circ$, 51367 reflections collected, 6446 unique ($R_{\text{int}} = 0.0479$, $R_{\text{sigma}} = 0.0335$), $R_1 = 0.0279$ ($I > 2\sigma(I)$), $wR_2 = 0.0655$ (all data).

Acknowledgments

This work was supported by Montana State University. Calculations were performed on the Extreme Science and Engineering Discovery Environment (XSEDE), which is supported by the NSF grant number ACI-1548562, using Comet at SDSC through allocation CHE-170089. NMR spectra were recorded on an instrument purchased with support from the NSF (NSF-MRI:DBI-1532078), the Murdock Charitable Trust Foundation (2015066:MNL), and MSU. X-ray crystallographic data were collected at the University of Montana X-ray diffraction core facility supported by the Center for Biomolecular Structure and Dynamics CoBRE (National Institutes of Health, CoBRE NIGMS P20GM103546). Single crystal X-ray diffraction data were collected using a Bruker D8 Venture, principally supported by NSF MRI CHE-1337908. We thank Daniel A. Decato for his assistance in solving crystal structures.

Appendix A. Supplementary data

Supplementary data to this article can be found online at <https://doi.org/10.1016/j.tet.2018.10.025>.

References

- [1] B.M. Rosen, K.W. Quasdorf, D.A. Wilson, N. Zhang, A.-M. Resmerita, N.K. Garg, V. Percec, *Chem. Rev.* 111 (2011) 1346–1416.
- [2] M. Tobisu, N. Chatani, *Top. Curr. Chem.* 374 (2016) 41.
- [3] V. Percec, J.Y. Bae, D.H. Hill, *J. Org. Chem.* 60 (1995) 1060–1065.
- [4] V. Percec, J.Y. Bae, D.H. Hill, *J. Org. Chem.* 60 (1995) 6895–6903.
- [5] D. Zim, V.R. Lando, J. Dupont, A.L. Monteiro, *Org. Lett.* 3 (2001) 3049–3051.
- [6] Z.Y. Tang, Q.S. Hu, *J. Am. Chem. Soc.* 126 (2004) 3058–3059.
- [7] V. Percec, G.M. Golding, J. Smidrkal, O. Weichold, *J. Org. Chem.* 69 (2004) 3447–3452.
- [8] Z.Y. Tang, S. Spinella, Q.S. Hu, *Tetrahedron Lett.* 47 (2006) 2427–2430.
- [9] D.A. Wilson, C.J. Wilson, B.M. Rosen, V. Percec, *Org. Lett.* 10 (2008) 4879–4882.
- [10] B.T. Guan, Y. Wang, B.J. Li, D.G. Yu, Z.J. Shi, *J. Am. Chem. Soc.* 130 (2008) 14468–14470.
- [11] K.W. Quasdorf, X. Tian, N.K. Garg, *J. Am. Chem. Soc.* 130 (2008) 14422–14423.
- [12] M. Tobisu, T. Shimasaki, N. Chatani, *Angew. Chem. Int. Ed.* 47 (2008) 4866–4869.
- [13] K.W. Quasdorf, M. Riener, K.V. Petrova, N.K. Garg, *J. Am. Chem. Soc.* 131 (2009) 17748–17749.
- [14] A. Antoft-Finch, T. Blackburn, V. Snieckus, *J. Am. Chem. Soc.* 131 (2009) 17750–17752.
- [15] C. Moldoveanu, D.A. Wilson, C.J. Wilson, P. Leowanawat, A.M. Resmerita, C. Liu, B.M. Rosen, V. Percec, *J. Org. Chem.* 75 (2010) 5438–5452.
- [16] P. Leowanawat, A.M. Resmerita, C. Moldoveanu, C. Liu, N. Zhang, D.A. Wilson, L.M. Hoang, B.M. Rosen, V. Percec, *J. Org. Chem.* 75 (2010) 7822–7828.
- [17] Y.L. Zhao, Y. Li, Y. Li, L.X. Gao, F.S. Han, *Chem. Eur. J.* 16 (2010) 4991–4994.
- [18] G.A. Molander, F. Beaumard, *Org. Lett.* 12 (2010) 4022–4025.
- [19] X.H. Fan, L.M. Yang, *Eur. J. Org. Chem.* (2010) 2457–2460.
- [20] B.T. Guan, X.Y. Lu, Y. Zheng, D.G. Yu, T. Wu, K.L. Li, B.J. Li, Z.J. Shi, *Org. Lett.* 12 (2010) 396–399.
- [21] H. Chen, Z. Huang, X. Hu, G. Tang, P. Xu, Y. Zhao, C.H. Cheng, *J. Org. Chem.* 76 (2011) 2338–2344.
- [22] P. Leowanawat, N. Zhang, A.M. Resmerita, B.M. Rosen, V. Percec, *J. Org. Chem.* 76 (2011) 9946–9955.
- [23] X.H. Fan, L.M. Yang, *Eur. J. Org. Chem.* (2011) 1467–1471.
- [24] C.H. Xing, J.R. Lee, Z.Y. Tang, J.R. Zheng, Q.S. Hu, *Adv. Synth. Catal.* 353 (2011) 2051–2059.
- [25] K.W. Quasdorf, A. Antoft-Finch, P. Liu, A.L. Silberstein, A. Komaromi, T. Blackburn, S.D. Ramgren, K.N. Houk, V. Snieckus, N.K. Garg, *J. Am. Chem. Soc.* 133 (2011) 6352–6363.
- [26] Y.L. Zhao, Y. Li, S.M. Li, Y.G. Zhou, F.Y. Sun, L.X. Gao, F.S. Han, *Adv. Synth. Catal.* 353 (2011) 1543–1550.
- [27] M. Baghbanzadeh, C. Pilger, C.O. Kappe, *J. Org. Chem.* 76 (2011) 1507–1510.
- [28] R. Kuwano, R. Shimizu, *Chem. Lett.* 40 (2011) 913–915.
- [29] P. Leowanawat, N. Zhang, V. Percec, *J. Org. Chem.* 77 (2012) 1018–1025.
- [30] P. Leowanawat, N. Zhang, M. Safi, D.J. Hoffman, M.C. Fryberger, A. George, V. Percec, *J. Org. Chem.* 77 (2012) 2885–2892.
- [31] N. Zhang, D.J. Hoffman, N. Gutsche, J. Gupta, V. Percec, *J. Org. Chem.* 77 (2012) 5956–5964.
- [32] G.J. Chen, F.S. Han, *Eur. J. Org. Chem.* (2012) 3575–3579.
- [33] N. Zhang, D.J. Hoffman, N. Gutsche, J. Gupta, V. Percec, *J. Org. Chem.* 77 (2012) 5956–5964.
- [34] R.L. Jezorek, N. Zhang, P. Leowanawat, M.H. Bunner, N. Gutsche, A.K.R. Pesti, J.T. Olsen, V. Percec, *Org. Lett.* 16 (2014) 6326–6329.
- [35] H. Ke, X. Chen, G. Zou, *J. Org. Chem.* 79 (2014) 7132–7140.
- [36] T. Xing, Z. Zhang, Y.X. Da, Z.J. Quan, X.C. Wang, *Tetrahedron Lett.* 56 (2015) 6495–6498.
- [37] J. Malineni, R.L. Jezorek, N. Zhang, V. Percec, *Synthesis* 48 (2016) 2795–2807.
- [38] J. Malineni, R.L. Jezorek, N. Zhang, V. Percec, *Synthesis* 48 (2016) 2808–2815.
- [39] A. Ohtsuki, K. Yanagisawa, T. Furukawa, M. Tobisu, N. Chatani, *J. Org. Chem.* 81 (2016) 9409–9414.
- [40] L. Guo, C.C. Hsiao, H. Yue, X. Liu, M. Rueping, *ACS Catal.* 6 (2016) 4438–4442.
- [41] M.M. Beromi, A. Nova, D. Balcells, A.M. Brasacchio, G.W. Brudvig, L.M. Guard, N. Hazari, D.J. Vinyard, *J. Am. Chem. Soc.* 139 (2017) 922–936.
- [42] E. Wenkert, E.L. Michelotti, C.S. Swindell, *J. Am. Chem. Soc.* 101 (1979) 2246–2247.
- [43] T. Hayashi, Y. Katsuro, Y. Okamoto, M. Kumada, *Tetrahedron Lett.* 22 (1981) 4449–4452.
- [44] S. Sengupta, M. Leite, D.S. Raslan, C. Quesnelle, V. Snieckus, *J. Org. Chem.* 57 (1992) 4066–4068.
- [45] J.W. Dankwardt, *Angew. Chem. Int. Ed.* 43 (2004) 2428–2432.
- [46] T.K. Macklin, V. Snieckus, *Org. Lett.* 7 (2005) 2519–2522.
- [47] P.M. Wehn, J. Du Bois, *Org. Lett.* 7 (2005) 4685–4688.
- [48] N. Yoshikai, H. Matsuda, E. Nakamura, *J. Am. Chem. Soc.* 131 (2009) 9590–9599.
- [49] B.T. Guan, X.Y. Lu, Y.Z. Zheng, D.G. Yu, T. Wu, K.L. Li, B.J. Li, Z.J. Shi, *Org. Lett.* 12 (2010) 396–399.
- [50] D.G. Yu, B.J. Li, S.F. Zheng, B.T. Guan, B.Q. Wang, Z.J. Shi, *Angew. Chem. Int. Ed.* 49 (2010) 4566–4570.
- [51] Z. Jin, Y.J. Li, Y.Q. Ma, L.L. Qiu, J.X. Fang, *Chem. Eur. J.* 18 (2012) 446–450.
- [52] C.A. Malapit, M.D. Visco, J.T. Reeves, C.A. Busacca, A.R. Howell, C.H. Senanayake, *Adv. Synth. Catal.* 357 (2015) 2199–2204.
- [53] X. Ye, Z. Yuan, Y. Zhou, Q. Yang, Y. Xie, Z. Deng, Y. Peng, *J. Heterocycl. Chem.* 53 (2016) 1956–1962.
- [54] B.J. Li, Y.Z. Li, X.Y. Lu, J. Liu, B.T. Guan, Z.J. Shi, *Angew. Chem. Int. Ed.* 47 (2008) 10124–10127.
- [55] C. Wang, T. Ozaki, R. Takita, M. Uchiyama, *Chem. Eur. J.* 18 (2012) 3482–3485.
- [56] J.L. Tao, Z.X. Wang, *Eur. J. Org. Chem.* (2015) 6534–6540.
- [57] A.R. Ehle, Q. Zhou, M.P. Watson, *Org. Lett.* 14 (2012) 1202–1205.
- [58] S.Z. Tasker, A.C. Gutierrez, T.F. Jamison, *Angew. Chem. Int. Ed.* 53 (2014) 1858–1861.
- [59] Y. Li, K. Wang, Y. Ping, Y. Wang, W. Kong, *Org. Lett.* 20 (2018) 921–924.
- [60] K. Muto, J. Yamaguchi, K. Itami, *J. Am. Chem. Soc.* 134 (2012) 169–172.
- [61] K. Amaike, K. Muto, J. Yamaguchi, K. Itami, *J. Am. Chem. Soc.* 134 (2012) 13573–13576.
- [62] J. Wang, D.M. Ferguson, D. Kalyani, *Tetrahedron* 69 (2013) 5780–5790.
- [63] K. Muto, T. Hatakeyama, J. Yamaguchi, K. Itami, *Chem. Sci.* 6 (2015) 6792.
- [64] Y. Wang, S.B. Wu, W.J. Shi, Z.J. Shi, *Org. Lett.* 18 (2016) 2548–2551.
- [65] D.A. Wilson, C.J. Wilson, C. Moldoveanu, A.M. Resmerita, P. Corcoran, L.M. Hoang, B.M. Rosen, V. Percec, *J. Am. Chem. Soc.* 132 (2010) 1800–1801.
- [66] K. Huang, D.G. Yu, S.F. Zheng, Z.H. Wu, Z.J. Shi, *Chem. Eur. J.* 17 (2011) 786–791.
- [67] G.A. Molander, L.N. Cavalcanti, C. García-García, *J. Org. Chem.* 78 (2013) 6427–6439.
- [68] C. Zarate, R. Manzano, R. Martin, *J. Am. Chem. Soc.* 137 (2015) 6754–6757.
- [69] L. Guo, M. Rueping, *Chem. Eur. J.* 22 (2016) 16787–16790.
- [70] J. Dong, H. Guo, Q.S. Hu, *Eur. J. Org. Chem.* (2017) 7087–7090.
- [71] F. Schoenebeck, K.N. Houk, *J. Am. Chem. Soc.* 132 (2010) 2496–2497.
- [72] F. Proutiere, F. Schoenebeck, *Angew. Chem. Int. Ed.* 50 (2011) 8192–8195.
- [73] F. Proutiere, E. Lyngvi, M. Aufiero, I.A. Sanhueza, F. Schoenebeck, *Organometallics* 33 (2014) 6879–6884.
- [74] For an experimental study using a bidentate phosphine see: S. Bajo, G. Laidlaw, A.R. Kennedy, S. Sproules, D.J. Nelson *Organometallics* 36 (2017) 1662–1672.
- [75] Z. Li, S.L. Zhang, Y. Fu, Q.X. Guo, L. Liu, *J. Am. Chem. Soc.* 131 (2009) 8815–8823.
- [76] L. Liu, S. Zhang, H. Chen, Y. Lv, J. Zhu, Y. Zhao, *Chem. Asian J.* 8 (2013) 2592–2595.
- [77] J. Cornellà, E. Gómez-Benoya, R. Martin, *J. Am. Chem. Soc.* 135 (2013) 1997–2009.
- [78] X. Hong, Y. Liang, K.N. Houk, *J. Am. Chem. Soc.* 136 (2014) 2017–2025.
- [79] K. Muto, J. Yamaguchi, D. Musaev, K. Itami, *Nat. Commun.* 5 (2015) 7508.
- [80] M.C. Schwarzer, R. Konno, T. Hojo, A. Ohtsuki, K. Nakamura, A. Yasutome, H. Takahashi, T. Shimasaki, M. Tobisu, N. Chatani, S. Mori, *J. Am. Chem. Soc.* 139 (2017) 10347–10358.
- [81] Z.K. Yang, C. Wang, M. Uchiyama, *Synlett* 28 (2017) 2565–2568.
- [82] A. Chatupheraphat, H.H. Liao, W. Srimontree, L. Guo, Y. Minenkov, A. Poater, L. Cavallo, M. Rueping, *J. Am. Chem. Soc.* 140 (2018) 3724–3735.
- [83] Review: Grimme, *WIREs Comput. Mol. Sci.* (2011) 211–228.
- [84] Energy calculations were performed with B3PW91, B3LYP, and B3PW91 for references [25,75 and 76], respectively.
- [85] Y. Zhao, D.G. Truhlar, *Org. Lett.* 9 (2007) 1967–1970.
- [86] D. Benitez, E. Tkatchouk, W.A. Goddard, *Chem. Commun.* (2008) 6194–6196.
- [87] C.L. McMullin, J. Jover, J.N. Harvey, N. Fey, *Dalton Trans.* 39 (2010) 10833–10836.
- [88] M.S.G. Ahlquist, P.O. Norrby, *Angew. Chem. Int. Ed.* 50 (2011) 11794–11797.
- [89] S.O.N. Lill, P. Ryberg, T. Rein, E. Bennström, P.O. Norrby, *Chem. Eur. J.* 18 (2012) 1640–1649.
- [90] C.L. McMullin, N. Fey, J.N. Harvey, *Dalton Trans.* 43 (2014) 13545.
- [91] J. Zhu, Y. Liang, L. Wang, Z.B. Zheng, K.N. Houk, Y. Tang, *J. Am. Chem. Soc.* 136 (2014) 6900–6903.
- [92] E. Lyngvi, I.A. Sanhueza, F. Schoenebeck, *Organometallics* 34 (2015) 805–812.
- [93] A.D. Becke, *Phys. Rev. A* 38 (1988) 3098–3100.
- [94] A.D. Becke, *J. Chem. Phys.* 98 (1993) 5648–5652.
- [95] A.D. Becke, *J. Chem. Phys.* 98 (1993) 1372–1377.
- [96] Y. Zhao, D.G. Truhlar, *J. Chem. Phys.* 125 (2006) 194101–194118.
- [97] T. Sperger, I.A. Sanhueza, I. Kalvet, F. Schoenebeck, *Chem. Rev.* 115 (2015) 9532–9586.
- [98] Y. Zhao, D.G. Truhlar, *Theor. Chem. Acc.* 120 (2008) 215–241.
- [99] J.D. Chai, M. Head-Gordon, *Phys. Chem. Chem. Phys.* 10 (2008) 6615–6620.
- [100] S. Grimme, J. Antony, S. Ehrlich, H. Krieg, *J. Chem. Phys.* 132 (2010) 154104–154119.
- [101] S. Grimme, S. Ehrlich, L. Goerigk, *J. Comput. Chem.* 32 (2011) 1456–1465.
- [102] J.P. Perdew, K. Burke, M. Ernzerhof, *Phys. Rev. Lett.* 77 (1996) 3865–3868.
- [103] An analogous TS involving interaction between Ni and N could not be located.
- [104] B.J.W. Maes, S. Verbeeck, T. Verhelst, A. Ekombie, N. von Wolff, G. Lefevre, E.A. Mitchell, A. Jutand, *Chem. Eur. J.* 21 (2015) 7858–7865.
- [105] H. Jacobsen, *Phys. Chem. Chem. Phys.* 11 (2009) 7231–7240.
- [106] T. Schwabe, S. Grimme, J.P. Djukic, *J. Am. Chem. Soc.* 131 (2009) 14156–14157.
- [107] A.A. Fokin, D. Gerbig, P.R. Schreiner, *J. Am. Chem. Soc.* 133 (2011) 20036–20039.
- [108] S. Grimme, P.R. Schreiner, *Angew. Chem. Int. Ed.* 50 (2011) 12639–12642.

- [109] P.R. Schreiner, L.V. Chernish, P.A. Gunchenko, E.Y. Tikhonchuk, H. Hausmann, M. Serafin, S. Schlecht, J.E.P. Dahl, R.M.K. Carlson, A.A. Fokin, *Nature* **407** (2011) 308–311.
- [110] A.A. Fokin, L.V. Chernish, P.A. Gunchenko, E.Y. Tikhonchuk, H. Hausmann, M. Serafin, J.E.P. Dahl, R.M.K. Carlson, P.R. Schreiner, *J. Am. Chem. Soc.* **134** (2012) 13641–13650.
- [111] S. Grimme, *Chem. Eur. J.* **18** (2012) 9955–9964.
- [112] A. Dieckmann, K.N. Houk, *J. Chem. Theor. Comput.* **8** (2012) 5064–5071.
- [113] S. Ehrlich, H.F. Bettinger, S. Grimme, *Angew. Chem. Int. Ed.* **52** (2013) 10892–10895.
- [114] B.D. Rekken, T.M. Brown, J.C. Fettinger, F. Lips, H.M. Tuononen, R.H. Herber, P.P. Power, *J. Am. Chem. Soc.* **135** (2013) 10134–10148.
- [115] D.A. Safin, M.G. Babashkina, K. Robeyns, M.P. Mitoraj, P. Kubisiak, Y. Garcia, *Chem. Eur. J.* **21** (2015) 16679–16687.
- [116] D.B. Ninkovic, S. Moncho, P.V. Petrovic, S.D. Zaric, M.B. Hall, E.N. Brothers, *J. Coord. Chem.* **69** (2016) 1759–1768.
- [117] K. Rohmann, M. Hölscher, W. Leitner, *J. Am. Chem. Soc.* **138** (2016) 433–443.
- [118] V.H. Menezes da Silva, A.P. de Lima Batista, O. Navarro, A.A.C. Braga, *J. Comput. Chem.* **38** (2017) 2371–2377.
- [119] M. Xie, W. Lu, *RSC Adv.* **8** (2018) 2240–2247.
- [120] G. Lu, R.Y. Liu, Y. Yang, C. Fang, D.S. Lambrecht, S.L. Buchwald, P. Liu, *J. Am. Chem. Soc.* **139** (2017) 16548–16555.
- [121] Review: J.P. Wagner, P.R. Schreiner *ACIE* **54** (2015) 12274–12296.
- [122] Review: D.J. Liptrot, P.P. Power *Nat. Rev. Chem.* **1** (2017) 0004.
- [123] H. Jacobsen, L. Cavallo, *ChemPhysChem* **13** (2012) 562–569.
- [124] I. Kobylanski, F.J. Widner, B. Kräutler, P. Chen, *J. Am. Chem. Soc.* **135** (2013) 13648–13651.
- [125] D. Roy, M. Marianski, N.T. Maitra, J.J. Dannenberg, *J. Chem. Phys.* **137** (2012), 134109.
- [126] Review: C.A. Fleckenstein, H. Plenio *Chem. Soc. Rev.* **39** (2010) 694–711.
- [127] U. Christmann, R. Vilar, *Angew. Chem. Int. Ed.* **44** (2005) 366–374.
- [128] Both B3LYP and M06L accurately predict that **12** is more stable than an analogous bis-phosphine ligated product $[(\text{PCy}_3)_2\text{Ni}(\text{Ar})(\text{OSO}_2\text{NMe}_2)]$ (see SI for details).
- [129] Only free phosphine is observed by ^{31}P NMR.
- [130] Displacement of cod by PCy_3 is endergonic: see Refs. [77,80].
- [131] Tobisu, Chatani, and Mori reached a similar conclusion for the reaction of methoxyarenes with $\text{Ni}(\text{P}^{\text{t}}\text{Bu}_3)$: see Ref. [80].
- [132] M.J. Frisch, et al., *Gaussian 09, Revision C.1*, Gaussian, Inc., Wallingford, CT, 2009 (see SI for full reference).
- [133] P.J. Hay, W.R. Wadt, *J. Chem. Phys.* **82** (1985) 299–310.
- [134] R.F. Ribeiro, A.V. Marenich, C.J. Cramer, D.G. Truhlar, *J. Phys. Chem. B* **115** (2011) 14556–14562.
- [135] C. Gonzalez, H.B. Schlegel, *J. Chem. Phys.* **90** (1989) 2154–2161.
- [136] C. Gonzalez, H.B. Schlegel, *J. Phys. Chem.* **94** (1990) 5523–5527.
- [137] K. Fukui, *Acc. Chem. Res.* **14** (1981) 363–368.
- [138] C. Krüger, Y.H. Tsay, *J. Organomet. Chem.* **34** (1971) 387–395.
- [139] M. Dolg, U. Wedig, H. Stoll, H. Preuss, *J. Chem. Phys.* **86** (1987) 866–872.
- [140] D. Andrae, U. Haussermann, M. Dolg, H. Stoll, H. Preuss, *Theor. Chim. Acta* **77** (1990) 123–141.
- [141] M. Cossi, N. Rega, G. Scalmani, V. Barone, *J. Comput. Chem.* **24** (2003) 669–681.
- [142] C.Y. Legault, CYLview, 1.0b, Université de Sherbrooke, 2009. <http://www.cylview.org>.
- [143] B.T. Guan, S.K. Xiang, B.Q. Wang, Z.P. Sun, Y. Wang, K.Q. Zhao, Z.J. Shi, *J. Am. Chem. Soc.* **130** (2008) 3268–3269.
- [144] G.M. Sheldrick, SADABS: Area Detector Absorption Correction, University of Göttingen, Germany, 1996.
- [145] O.V. Dolomanov, L.J. Bourhis, R.J. Gildea, J.A.K. Howard, H. Puschmann, *J. Appl. Crystallogr.* **42** (2009) 339–341.
- [146] G.M. Sheldrick, *Acta Crystallogr. A* **71** (2015) 3–8.
- [147] G.M. Sheldrick, *Acta Crystallogr. C* **71** (2015) 3–8.
- [148] Bruker, APEX3, Bruker AXS Inc., Madison, Wisconsin, USA, 2016.
- [149] G.M. Sheldrick, *Acta Crystallogr. A* **64** (2008) 112–122.